# Electronic Supplementary Information (ESI) for:

# An Endohedral Titanium (III) in a Clusterfullerene: Putting a Non-Group-III Metal Nitride into the $C_{80}$-$I_h$ Fullerene Cage

Shangfeng Yang, *[a] Chuanbao Chen,[a] Alexey A. Popov,[b] Wenfeng Zhang,[a] Fupin Liu,[a] and Lothar Dunsch [b]

[a] *Hefei National Laboratory for Physical Sciences at Microscale & Department of Materials Science and Engineering, University of Science and Technology of China (USTC), Hefei 230026, China*

[b] *Group of Electrochemistry and Conducting Polymers, Leibniz-Institute for Solid State and Materials Research (IFW) Dresden, D-01171 Dresden, Germany*

## Contents

### *S1. Synthesis and measurements of $TiSc_2N@C_{80}$*

A mixture of $TiO_2$ (99.99%) and $Sc_2O_3$ (99.99%) and graphite powder with a certain Ti:Sc molar ratio which was variable from 8:1 to 1:2 (typically 1:1, molar ratio of Sc:C is fixed at 1:15) was subjected for DC-arc discharging by a modified Krätschmer-Huffman DC-arc discharging method with the addition of $N_2$ (10 mbar) into 400 mbar He. The as-produced soot was Soxhlet-extracted by $CS_2$ for 24 h, and the resulting brown-yellow solution was distilled to remove $CS_2$ and then immediately redissolved in toluene (~ 200 ml) and subsequently passed through a 0.2 μm Telflon filter (Sartorius AG, Germany) for HPLC separation. The separation of $TiSc_2N@C_{80}$ was performed by multistep HPLC as described in details in S3. The purity of the isolated $TiSc_2N@C_{80}$ was further checked by LD-TOF MS analysis running in both positive and negative ion modes (Autoflex III, Bruker Daltonics Inc., Germany). UV-vis-NIR spectra of $TiSc_2N@C_{80}$ dissolved in toluene were recorded on a UV-Vis-NIR 3600 spectrometer (Shimadzu, Japan) using quartz cell of 1 mm layer thickness and 1 nm resolution. For FTIR measurements of $TiSc_2N@C_{80}$, the sample was drop-coated onto KBr single crystal disks. The residual toluene was removed by heating the polycrystalline films in a vacuum of $2 \times 10^{-6}$ mbar at 235 °C for 3 h. The FTIR spectrum was recorded at room temperature on an IFS 66v spectrometer (Bruker, Germany). The $^{13}C$ NMR spectroscopic study was performed at 125 MHz in a multiprobe head PH 1152Z of an Avance 500 spectrometer (Bruker) at room temperature in carbon disulfide solutions with $d_6$-acetone as a lock. For XPS measurements, thin films of $TiSc_2N@C_{80}$ drop-coated onto KBr single crystal disks were transferred under ultrahigh vacuum conditions into an ESCALAB 250 spectrometer (Thermo-VG Scientific, England) where they were studied using monochromatic Al $K_\alpha$ radiation (1486.6 eV) with an energy resolution of 0.6 eV.

### *S2. Comparison of LD-TOF MS spectra of the fullerene extract mixtures synthesized from $TiO_2/Sc_2O_3$ with $N_2$ addition and $TiO_2$ with $N_2$ addition*

As discussed in the text in details, the fullerene extract mixtures synthesized from $TiO_2/Sc_2O_3$ with $N_2$ addition ($TiO_2/Sc_2O_3$ extract) and $TiO_2$ with $N_2$ addition ($TiO_2$ extract) were prepared by a modified Krätschmer-Huffman DC-arc discharging method using $TiO_2/Sc_2O_3$ and $TiO_2$ as the raw material, respectively. Figure S1 compared the LD-TOF MS spectra of these two extracts and the assignments of each mass peaks in the region of m/z=1050-1160 are listed in Table S1, indicating clearly that no Ti-containing NCFs was formed in the $TiO_2$ extract.

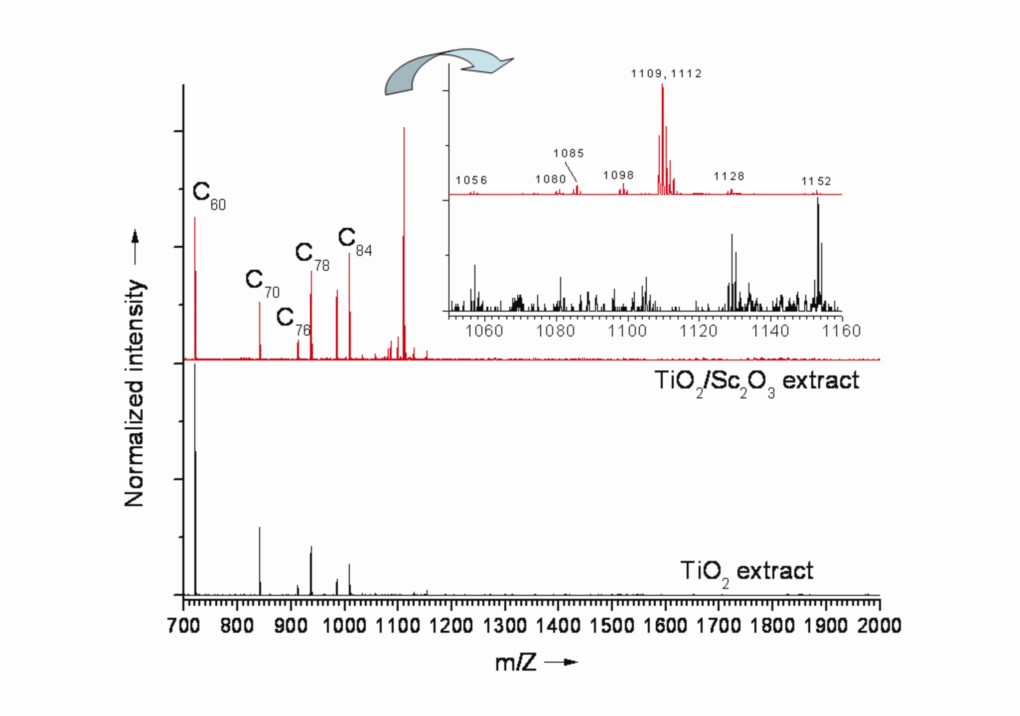

**Fig. S1.** Positive ion laser desorption time-of-flight (LD-TOF) mass spectra of the $TiO_2/Sc_2O_3$ and $TiO_2$ extracts with $N_2$ addition. The insets show the enlarged region of m/z=1050-1160 (the intensity of $TiO_2/Sc_2O_3$ extracts is divided 10 times for clarity).

**Table S1**. Assignments of the characteristic mass peaks (m/z=1050-1160) of the $TiO_2/Sc_2O_3$ and $TiO_2$ extracts.

<table>
<tr><td rowspan="4">$TiO_2/Sc_2O_3$ extract</td><td>m/z</td><td colspan="2">1056</td><td colspan="2">1080</td><td colspan="2">1085</td><td colspan="2">1098</td></tr>
<tr><td>components</td><td colspan="2">$C_{88}$, $Ti_2C_{80}$</td><td colspan="2">$C_{90}$, $Ti_2C_{82}$</td><td colspan="2">$Sc_3N@C_{78}$</td><td colspan="2">$TiSc_2@C_{80}$</td></tr>
<tr><td>m/z</td><td colspan="2">1109</td><td colspan="2">1112</td><td colspan="2">1128</td><td colspan="2">1152</td></tr>
<tr><td>components</td><td colspan="2">$Sc_3N@C_{80}$</td><td colspan="2">$TiSc_2N@C_{80}$</td><td colspan="2">$C_{94}$, $Ti_2C_{86}$,<br>$Ti@C_{90}$</td><td colspan="2">$C_{96}$, $Ti_2C_{88}$</td></tr>
<tr><td rowspan="2">$TiO_2$ extract</td><td>m/z</td><td>1056</td><td colspan="2">1080</td><td colspan="2">1104</td><td colspan="2">1128</td><td>1152</td></tr>
<tr><td>components</td><td>$C_{88}$,<br>$Ti_2C_{80}$</td><td colspan="2">$C_{90}$,<br>$Ti_2C_{82}$</td><td colspan="2">$C_{92}$,<br>$Ti_2C_{84}$</td><td colspan="2">$C_{94}$,<br>$Ti_2C_{86}$, $Ti@C_{90}$</td><td>$C_{96}$,<br>$Ti_2C_{88}$</td></tr>
</table>

### *S3. Isolation of $TiSc_2N@C_{80}$:*

Figure S2 compares the LD-TOF MS spectra of the two subfractions A1 and A2, indicating that subfractions A1 contains only $Sc_3N@C_{80}$ (I, $I_h$) whereas an additional mass peak of 1112 ($TiSc_2N@C_{80}$) exists in the subfractions A2.

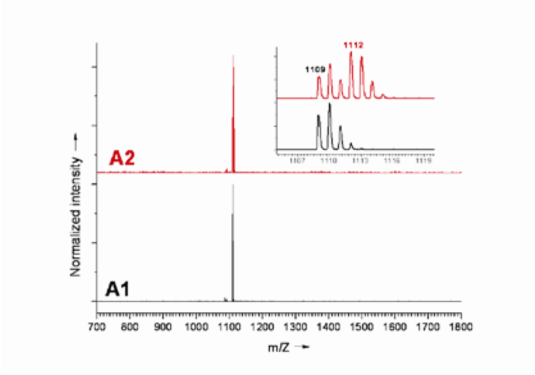

**Fig. S2.** Positive ion laser desorption time-of-flight (LD-TOF) mass spectra of the subfractions A1 and A2.

Subfraction A2 is collected and subjected to two-step recycling HPLC isolation resulting in the isolation of $TiSc_2N@C_{80}$. In the first-step HPLC isolation running in 10 x 250 mm Buckyprep columns (Figure S3), three fractions are collected after two cycles. LD-TOF MS spectroscopic measurements and the comparison of the HPLC chromatogram to that of $Sc_3N@C_{80}$ ($I_h$ + $D_{5h}$) indicate that fractions A2-1 and A2-2 are correlated to $Sc_3N@C_{80}$ (I, $I_h$) and $Sc_3N@C_{80}$ (II, $D_{5h}$), respectively, whereas fraction A2-3 comprises of two mass peaks at 1109 and 1112 (see Table S2).

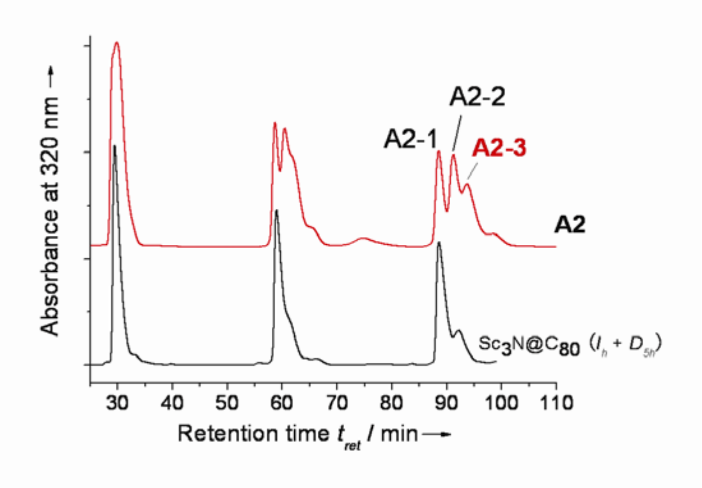

**Fig. S3.** Recycling HPLC chromatograms of the subfraction A2 of $TiO_2/Sc_2O_3$ extract in comparison with that of $Sc_3N@C_{80}$ ($I_h$ + $D_{5h}$) which is obtained from fraction A of the pure $Sc_2O_3$ extract. (10 x 250 mm Buckyprep column; flow rate 5.0 ml/min; injection volume 5 ml; toluene as eluent; 25°C). A2-1: $Sc_3N@C_{80}$ (I, $I_h$), A2-2: $Sc_3N@C_{80}$ (II, $D_{5h}$), A2-3: $TiSc_2N@C_{80}$ + $Sc_3N@C_{80}$ (II, $D_{5h}$).

The collected subfraction A2-3 is then subjected for the second-step recycling HPLC running in a Buckyprep-M column and the chromatogram is shown in Fig. S4. After two cycles, the residual subfraction A2-3-1 ($Sc_3N@C_{80}$ (II, $D_{5h}$)) as well as other residual empty fullerenes ($t_{ret}$ < 30 min in the first cycle) is successfully removed and a pure fraction A2-3-2 is collected. Fraction A2-3-2 is then measured by LD-TOF MS spectroscopy, confirming its chemical composition and purity (see Fig. S5 and Table S2).

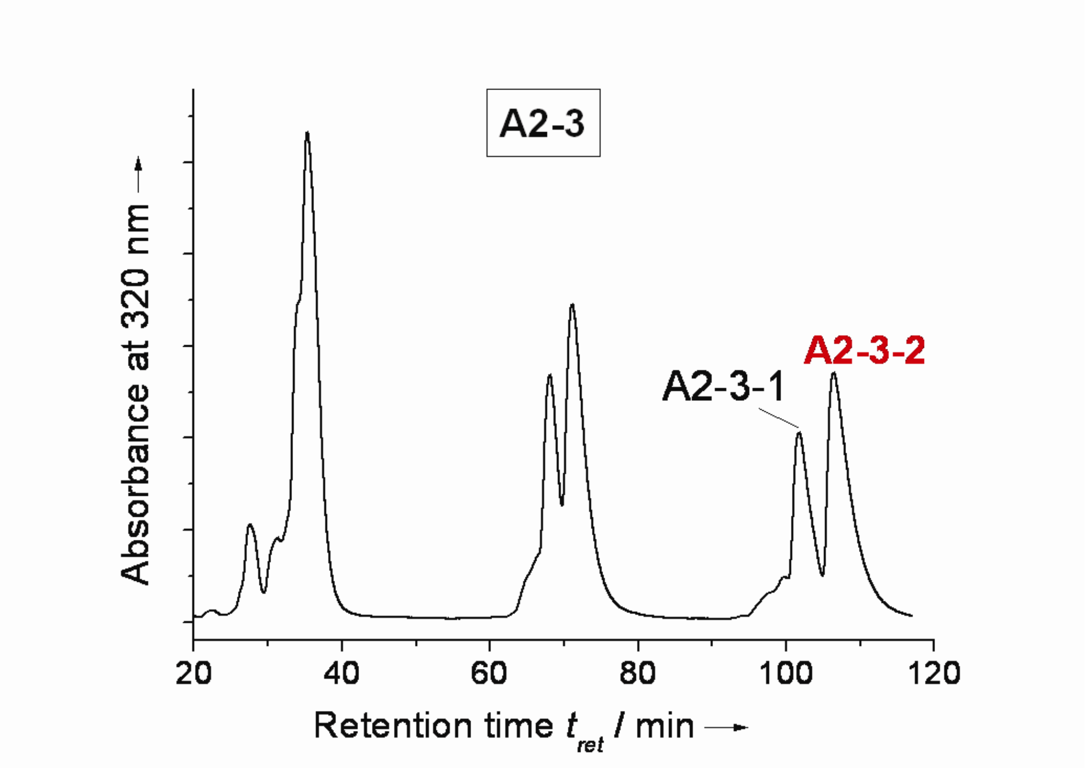

**Fig. S4.** Recycling HPLC chromatograms of the isolated subfraction A2-3 (10 x 250 mm Buckyprep-M column; flow rate 5.0 ml/min; injection volume 6 ml; toluene as eluent; 25°C). The peaks with $t_{ret}$ < 30 min in the first cycle are due to the residual empty fullerenes ($C_{86}$, $C_{88}$ etc). A2-3-1: $Sc_3N@C_{80}$ (II, $D_{5h}$), A2-3-2: $TiSc_2N@C_{80}$.

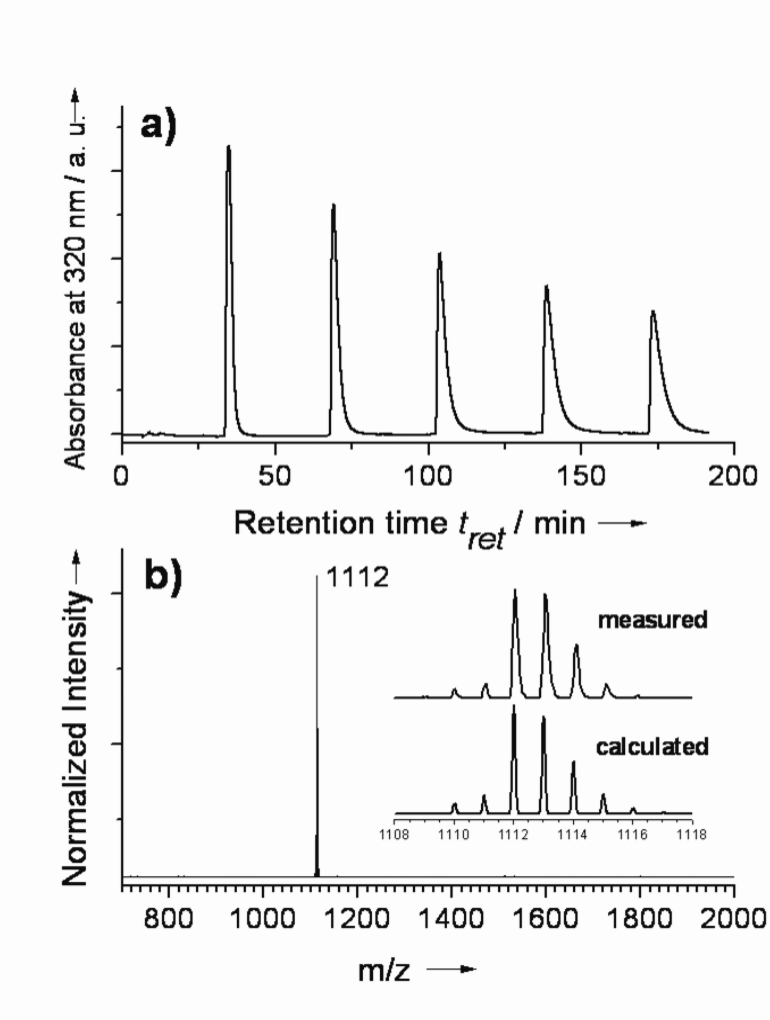

**Fig. S5.** a) Recycling HPLC chromatogram of $TiSc_2N@C_{80}$ in four cycles (10 x 250 mm Buckyprep-M column; flow rate 3.0 ml/min; injection volume 6 ml; toluene as eluent; 25°C). b) Positive ion laser desorption time-of-flight (LD-TOF) mass spectrum of $TiSc_2N@C_{80}$. The inset shows the measured and calculated isotope distributions of $TiSc_2N@C_{80}$.

## *S4. Determination of the optimized synthesis condition for the synthesis of $TiSc_2N@C_{80}$ and estimation of the relative yield of $TiSc_2N@C_{80}$ to those of $Sc_3N@C_{80}$ (I) and $Sc_3N@C_{80}$ (II)*:

Figure S6 shows the comparison of the HPLC chromatograms of the $TiO_2/Sc_2O_3$ extracts obtained with different molar ratio of Ti:Sc (8:1, 4:1, 2:1, 1:1, 1:2). Clearly the intensity of fractions A1 and A2 depends sensitively on the molar ratio of Ti:Sc. With the increase of the molar of Ti:Sc from 1:1 to 4:1, obviously the intensities of both fraction A1 and A2 decrease dramatically, suggesting that Ti metal may suppress the formation of Sc-based homogeneous NCFs as discussed in the text. When a molar ratio of Ti:Sc=8:1 is used, both fraction A1 and A2 disappears, indicating that no

NCF forms at all. On the other hand, if the molar of Ti:Sc of 1:2 is used, the intensities of both fraction A1 and A2 increase clearly. However, it should be noted that such an increase in intensity is largely due to the enhancement of the yield of $Sc_3N@C_{80}$ (I, II) instead of the $TiSc_2N@C_{80}$. Therefore, to determine the optimized synthesis condition for the synthesis of $TiSc_2N@C_{80}$, the absolute yield of $TiSc_2N@C_{80}$ in the extract mixture obtained under different molar ratio of Ti:Sc should be considered. Assuming that the abundance of $TiSc_2N@C_{80}$ in fraction A2 is constant, the relative yield of fraction A2 to A1 could be used to estimate the abundance of $TiSc_2N@C_{80}$ in the extract mixture.

The inset of Figure S6 shows the effect of the molar ratio of Ti:Sc on the peak area ratio of fraction A2:A1 (i.e. relative yield of fraction A2 to A1) for the extract mixture obtained under molar ratio of Ti:Sc of 1:2, 1:1 and 2:1 (the other ratios (4:1, 8:1) are not considered because of the significantly decreased intensity of fractions A1 and A2). Clearly a maximum of the peak area ratio of fraction A2:A1 is obtained at molar ratio of 1:1 (Ti:Sc), indicating that the highest abundance of $TiSc_2N@C_{80}$ in the extract mixture is obtained under this condition.

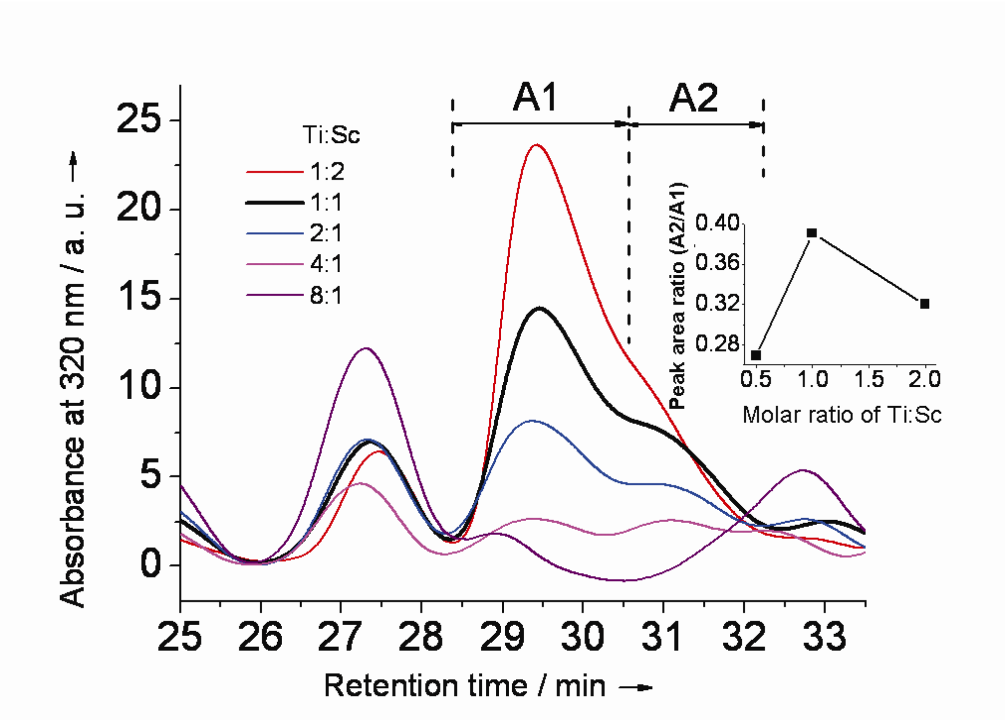

**Fig. S6.** HPLC chromatograms of the $TiO_2/Sc_2O_3$ extracts obtained with different molar ratio of Ti:Sc (10 x 250 mm Buckyprep column; flow rate 5.0 ml/min; injection volume 5 ml; toluene as eluent; 25°C). The inset shows the effect of the molar ratio of Ti:Sc on the peak area (integrated area of the HPLC peak) ratio of fraction A2:A1.

**_S5. Estimation of the relative yield of $TiSc_2N@C_{80}$ to those of $Sc_3N@C_{80}$ (I) and $Sc_3N@C_{80}$ (II)_:**

The relative yield of each fraction shown in Figs. 1, S3, S4, S5 is estimated based on the integrated area of the corresponding peak in the chromatogram, the results are summarized in Table S2.

**Table S2**. Assignments of each (sub)fraction and their relative yield and abundance

| fraction | subfraction | product | relative yield | relative abundance |
|---|---|---|---|---|
| A | A1 | $Sc_3N@C_{80}$ (I) | 4.44:1 (A1:A2) | 81.6% |
|  | A2 | $Sc_3N@C_{80}$ (I) + $Sc_3N@C_{80}$ (II) + TiSc2N@C80 |  | 18.4% |
| A2 | A2-1 | $Sc_3N@C_{80}$ (I) | 0.92:1.08:1 (A2-1:A2-2:A2-3) | 30.6% |
|  | A2-2 | $Sc_3N@C_{80}$ (II) |  | 36.1% |
|  | A2-3 | $Sc_3N@C_{80}$ (II) + TiSc2N@C80 |  | 33.3% |
| A2-3 | A2-3-1 | $Sc_3N@C_{80}$ (II) | 0.57:1 (A2-3-1:A2-3-2) | 36.5% |
|  | A2-3-2 | TiSc2N@C80 |  | 63.5% |

(1) The relative abundance of TiSc2N@C80 can be directly calculated as the subfraction A2-3-2:

$18.4\% \times 33.3\% \times 63.5\% \approx 3.89\ \%$

(2) To calculate the relative abundance of $Sc_3N@C_{80}$ (I) in the entire fraction A, the subfraction A1 and A2-1 must be considered:

$81.6\% + 18.4\% \times 30.6\% \approx 87.2\ \%$

(3) To calculate the relative abundance of $Sc_3N@C_{80}$ (II) in the entire fraction A, the subfraction A2-2 and A2-3-1 must be considered:

$18.4\% \times 36.1\% + 18.4\% \times 33.3\% \times 36.5\% \approx 8.88\ \%$

Therefore, the relative yield of TiSc2N@C80:Sc3N@C80 (I): Sc3N@C80 (II) is

$3.89\%: 87.2\%: 8.88\% \approx 1: 22.4: 2.3$

### *S6. Electrochemical study and cyclic voltammogram of TiSc$_2$N@C$_{80}$:*

Electrochemical studies of TiSc$_2$N@C$_{80}$ were performed in *o*-DCB solution. The supporting electrolyte was tetrabutylamonium hexafluorophosphate (TBAPF$_6$, puriss. electrochemical grade, Fluka) which was dried under pressure at 340 K for 24 h and stored in glove box prior to use. Cyclic voltammogram experiments were performed with a PAR 273 potentiostat (EG&G, US) at room temperature in a glove box. A standard three-electrode arrangement of a platinum (Pt) wire as working electrode, a platinum coil as counter electrode, and a silver wire as a pseudo-reference electrode was used. In a comparison experiment, ferrocene (Fc) was added as the internal standard and all potentials are referred to Fc/Fc$^+$ couple.

According to the cyclic voltammogram study, TiSc$_2$N@C$_{80}$ exhibits one reversible oxidation and three reversible reduction steps at +0.16, -0.94, -1.58, -2.21 V vs Fc/Fc$^+$. The electrochemical gap as the difference of the first reduction and oxidation potentials is calculated to be 1.10 V.

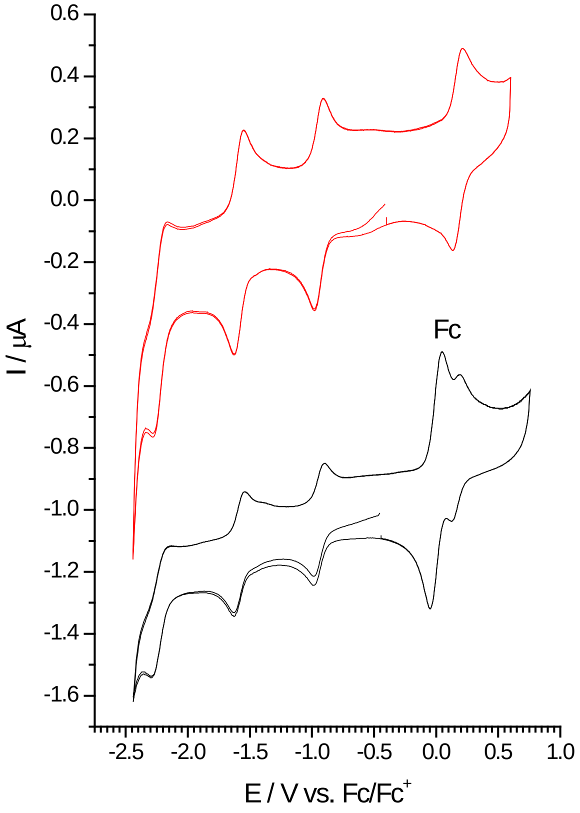

**Figure S7.** Cyclic voltammogram of pure TiSc$_2$N@C$_{80}$ (upper curve) and TiSc$_2$N@C$_{80}$/Fc mixture (lower curve) in *o*-DCB solution, scan rate: 20 mV/s, TBAPF$_6$ as supporting electrolyte. Note that the curve of TiSc$_2$N@C$_{80}$/Fc mixture (lower curve) was shifted downwards for clarity.

### *S7. ESR spectroscopic analysis of TiSc$_2$N@C$_{80}$:*

The ESR spectra of TiSc$_2$N@C$_{80}$ were measured in toluene solution using a Bruker Elexys 580 FT-EPR X-band spectrometer (9.5 GHz). Very broad featureless signal was found at the room temperature, while with the decrease of the temperature the gradual decrease of the bandwidth and increase of the signal intensity were observed.

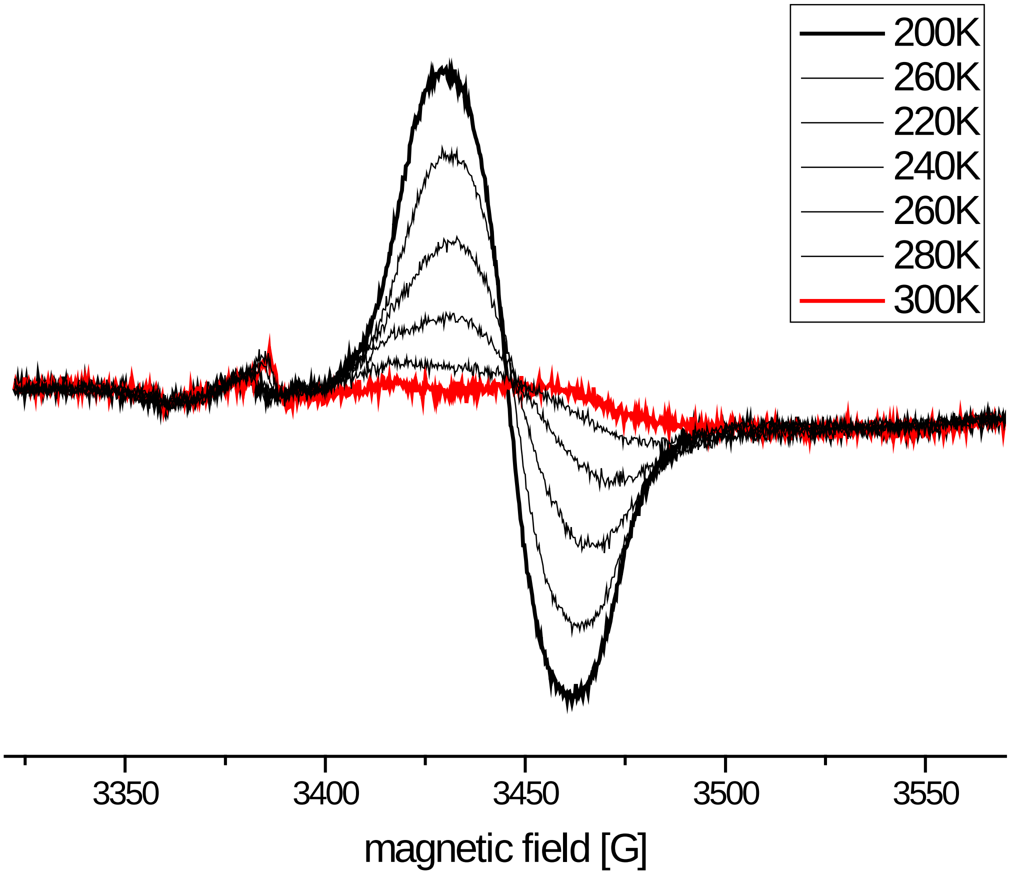

**Figure S8.** ESR spectra of TiSc$_2$N@C$_{80}$ in toluene under different measurement temperatures.

## ***S8. XPS spectroscopic analysis of $TiSc_2N@C_{80}$:***

Figure S9 shows the XPS spectra of the 2p levels of Ti and Sc in $TiSc_2N@C_{80}$, which may give a tentative direct determination of the valencies of Ti and Sc. The observed Ti $2p_{3/2}$ and $2p_{1/2}$ binding energies in $TiSc_2N@C_{80}$ are 455.7, 461.3 eV (Figure S9a), respectively. Comparing to the Ti $2p_{3/2}$ binding energies of other Ti-containing compounds in which Ti has a valence state ranging from 0 (454.1 eV in Ti) to 4 (e.g. 458.8 eV in $TiO_2$), the observed Ti $2p_{3/2}$ binding energy in $TiSc_2N@C_{80}$ (455.7 eV) is close to that in TiN in which Ti takes a valence state of 3 (Figure S9c[S1]), suggesting that the valence state of Ti in $TiSc_2N@C_{80}$ is 3.

Likewise, given that the observed Sc $2p_{3/2}$ binding energy in $TiSc_2N@C_{80}$ (400.7 eV, see Figure S9b) is close to that in ScN in which Sc takes a valence state of 3 (Figure S9d[S1]), the valence state of Sc in $TiSc_2N@C_{80}$ is 3 which is similar to that in $Sc_3N@C_{80}$ (I)[S2].

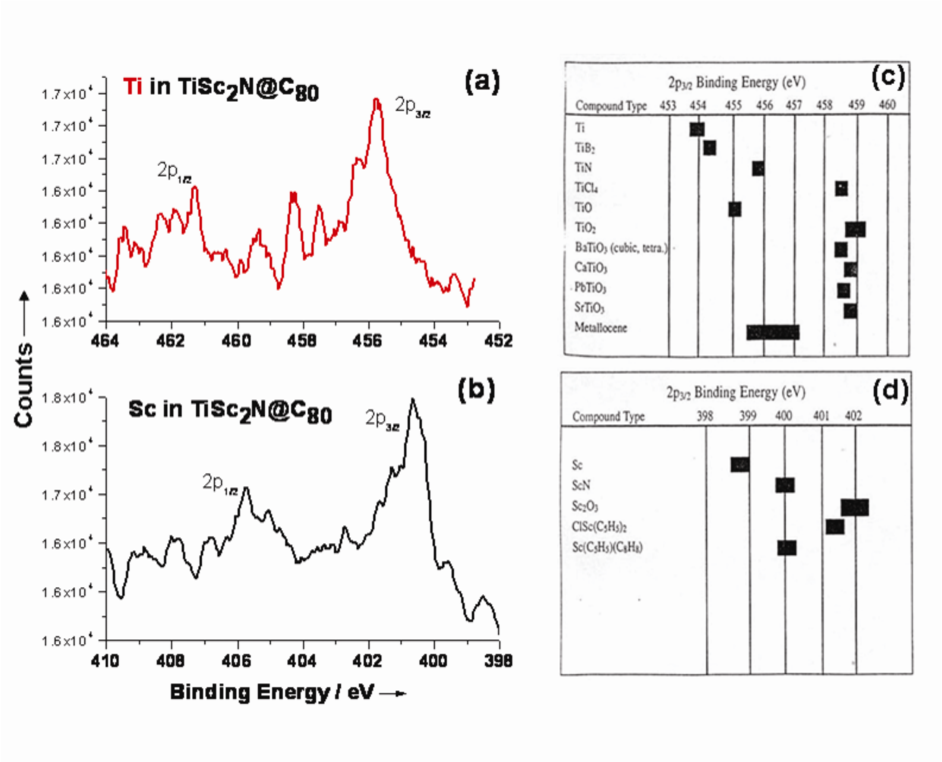

**Fig. S9.** XPS spectra of the 2p levels of Ti (a) and Sc (b) in $TiSc_2N@C_{80}$ (monochromatic Al $K_\alpha$ radiation (1486.6 eV), energy resolution: 0.6 eV). (c-d) Lists of the $2p_{3/2}$ binding energies of Ti and Sc in the corresponding compounds[S1].

### ***S9. Calculation results of $TiSc_2N@C_{80}$:***

There are several conformers of $Sc_3N@C_{80}$-$I_h$, among them the lowest energy is the $C_3$-conformer. At the same time, for the $Sc_3N@C_{80}^-$ radical-anion (which is isoelectronic to $TiSc_2N@C_{80}$), the conformer with $C_{3v}$ symmetry was found to be considerably more stable (see Fig. S10). Our calculations for different conformers of $TiSc_2N@C_{80}$ have also shown that the conformer of $TiSc_2N@C_{80}$ based on the $C_{3v}$-$Sc_3N@C_{80}$ (for $TiSc_2N@C_{80}$ it has $C_s$ symmetry) is more stable than the structure derived from $C_3$-conformer, however two conformer based on $C_s$-$Sc_3N@C_{80}$ are almost isoenergetic.

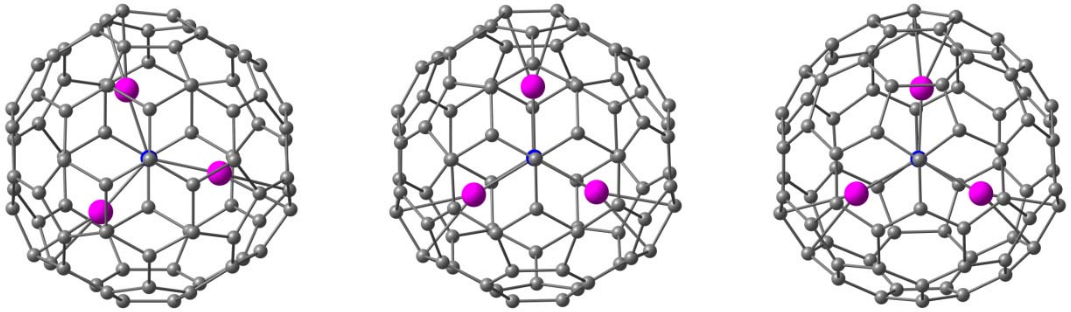

$C_3$, 0.0 (13.4) kJ/mol $C_{3v}$, 8.9 (0.0) kJ/mol $C_s$, 4.8 (2.3) kJ/mol

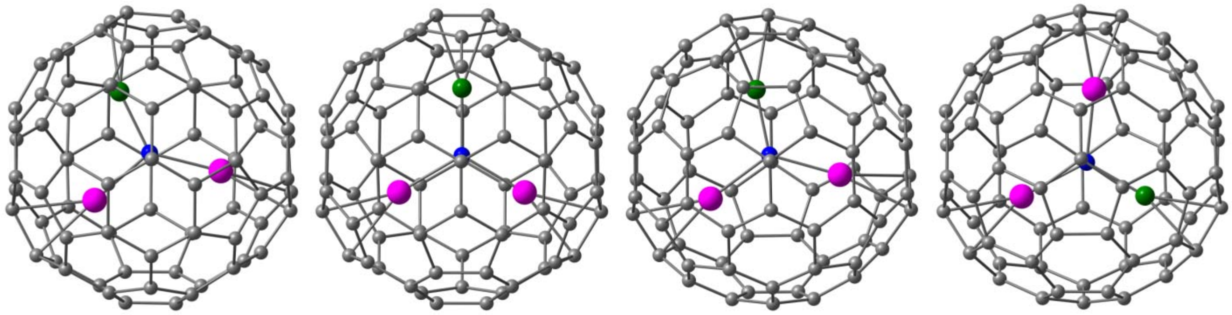

"$C_3$", 13.2 kJ/mol $C_s$ ("$C_{3v}$") 0.3 kJ/mol "$C_s$"-I, 0.8 kJ/mol $C_s$"-II, 0.0 kJ/mol

**Fig. S10.** Molecular structures of different conformers of $Sc_3N@C_{80}$ (top) and $Sc_2TiN@C_{80}$ (bottom) optimized at the PBE/TZ2P level. The relative energies of the conformers are given below each structure. For $Sc_3N@C_{80}$, the values in parentheses are relative energies for the radical anion ($Sc_3N@C_{80}^-$). The Ti, Sc, N atoms are drawn in green, purple, and blue, respectively.

### *S10. Analysis of the anti-symmetric M−N stretching modes of $TiSc_2N@C_{80}$*

It is known that the anti-symmetric M–N stretching vibrational modes ($\nu_{M\text{-}N}$) in NCFs, which appear as the most intense low-energy IR lines in the region of 600-800 $cm^{-1}$, are sensitively dependent on the encaged metal.[1-5,8-10,19] Opposite to the homogeneous NCFs, in which the anti-symmetric M–N stretching mode is two -fold degenerated, the lower molecular symmetry in MMNCFs results in the splitting of this mode as already revealed in the previous studies of $M_xSc_{3-x}N@C_{80}$ MMNCFs (M= Y, Ce, Gd, Tb, Dy, Er, Lu).[1,8,9] With respect to $TiSc_2N@C_{80}$ ($I_h$), it is found that these modes ($\nu_{Sc\text{-}N}$ and $\nu_{Ti\text{-}N}$) experience a similar splitting with two main components at 504 and 606 $cm^{-1}$, which can be assigned to $\nu_{Sc\text{-}N}$ and $\nu_{Ti\text{-}N}$ respectively according to DFT calculations. It should be noted that the $\nu_{Sc\text{-}N}$ mode of $TiSc_2N@C_{80}$ ($I_h$) (504 $cm^{-1}$) experiences a significant upshift to 599 $cm^{-1}$ in $Sc_3N@C_{80}$ (I, $I_h$) and 595 $cm^{-1}$ in $Sc_3N@C_{80}$ (II, $D_{5h}$,).[19] This is caused by the elongation of the Sc–N bonds in $TiSc_2N$ cluster (*ca* 2.08 Å) as compared to that in $Sc_3N$ cluster (2.018 Å). On the other hand, the DFT-predicted bondlength of Ti–N in $TiSc_2N@C_{80}$ is *ca* 1.92 Å.

## References

**[S1].** J. F. Moulder, W. F. Stickle, P. E. Sobol, K. D. Bomben, *Handbook of X-ray Photoelectron Spectroscopy*, Perkin-Elmer Corp., Eden Prairie, MN, USA, 1992.

**[S2].** L. Alvarez, T. Pichler, P. Georgi, T. Schwieger, H. Peisert, L. Dunsch, Z. Hu, M. Knupfer, J. Fink, P. Bressler, M. Mast, M. S. Golden, *Phys. Rev. B* **2002**, *66*, 035107.